Technical Report No. 216

036040-9-T

MODULATION BY LINEAR-MAXIMAL SHIFT REGISTER SEQUENCES: AMPLITUDE, BIPHASE AND COMPLEMENT-PHASE MODULATION

by

Theodore G. Birdsall
Richard M. Heitmeyer
Kurt Metzger

COOLEY ELECTRONICS LABORATORY

Department of Electrical and Computer Engineering
The University of Michigan
Ann Arbor, Michigan

for

Contract No. N00014-67-A-0181-0032
Office of Naval Research
Department of the Navy
Arlington, Virginia 22217

December 1971

ABSTRACT

This report describes the use of linear-maximal shift-register sequences either to amplitude modulate (AM) or to angle modulate a sinusoidal carrier. Two cases of angle modulation are considered: biphase modulation (BM) and complement-phase modulation (CM). In biphase modulation the carrier angle switches between $+\pi/2$ and $-\pi/2$, whereas in complement-phase modulation the carrier angle switches between $+\pi/4$ and $-\pi/4$. It is shown that the ratio of the average power to the peak power for AM is only one-half as large as for either BM or CM. On the other hand, the ratio of the carrier power to the average power for either AM or CM is one-half, but for BM this ratio is approximately zero. Finally, a replica-correlation technique for use with any of the three modulations is described.

ACKNOWLEDGMENT

The techniques described in this report have been developed for use in the project MIMI (University of Michigan - University of Miami) underwater-sound-propagation experiments sponsored by Code 468 of the Office of Naval Research.

TABLE OF CONTENTS

	Page
ABSTRACT	iii
ACKNOWLEDGMENT	iv
LIST OF ILLUSTRATIONS AND TABLES	vi
1. INTRODUCTION	1
2. A REVIEW OF LINEAR-MAXIMAL SHIFT-REGISTER SEQUENCES	3
3. AMPLITUDE MODULATION, BIPHASE MODULATION AND COMPLEMENT-PHASE MODULATION	8
4. A REPLICA-CORRELATION TECHNIQUE	17
APPENDIX	23
REFERENCES	27
DISTRIBUTION LIST	28

to construct a signal that has the same peak power, and effectively the same duty cycle, as the repeated pulse signal but with a larger average power. One such technique, which has gained in popularity since the advent of digital circuitry, involves the use of linear-maximal shift-register (LMSR) sequences to modulate the carrier. The transmitted signal is constructed to have a sufficiently large average-power to peak-power ratio while, at the receiver, the reception is correlated with a replica in order to achieve the effect of a small duty cycle.

This report describes three different LMSR modulation techniques that have been used in the MIMI (University of Michigan - University of Miami) underwater sound propagation experiments. Section 2 briefly reviews the linear-maximal, shift-register sequences. Section 3 describes the modulation techniques themselves and derives the power spectra for each case. In Section 4, a replica-correlation technique for achieving the effect of a small duty cycle is described. In large part the material contained in this report is taken from "MIMI Processing Techniques" (Ref. 1).

2. A REVIEW OF LINEAR-MAXIMAL, SHIFT-REGISTER SEQUENCES

A LMSR sequence $\{m_k\}$ is a periodic, binary sequence $m_k \in \{0, 1\}$, which can be generated by certain shift-register generators using mod-2 arithmetic. Methods of generating these sequences and their algebraic properties have been studied extensively (Refs. 2 and 3). Here only the following three properties are presented:

1. Periodic Property

The period L of a LMSR sequence is of the form

$$L = 2^n - 1 \qquad n = 1, 2, \ldots$$

The number n can be associated with the number of stages in the shift-register generator.

2. Balance Property

The total number of 1's in one period of an LMSR sequence is

$$(L+1)/2 = 2^{n-1}$$

and the total number of 0's is

$$(L-1)/2 = 2^{n-1} - 1$$

3. Pseudo-Random Property

The occurrence of 1's and 0's in an LMSR sequence has the appearance of having been generated by successive trials of a fair-coin tossing experiment. (A more precise statement of the pseudo-random property can be found in Ref. 2.)

The above three properties state (i) that LMSR sequences can only have periods of the form $L = 2^n - 1$, (ii) that there are approximately an equal number of 1's and -1's in an LMSR sequence, and (iii) that the order in which the 1's and 0's occur does not follow a simple pattern. A specific example of an LMSR sequence from a 4-stage generator, $n = 4$, with period, $L = 2^4 - 1 = 15$, is

$$\ldots\ 1\ 1\ 1\ 1\ 0\ 0\ 0\ 1\ 0\ 0\ 1\ 1\ 0\ 1\ 0\ \ldots\ .$$

In order to describe the use of LMSR sequences in modulation schemes, it is convenient to introduce the notion of the associated binary waveform. Basically, the idea is to construct a periodic, binary-valued function of time, m(t), by associating logical 1's in $\{m_k\}$ with +1 values of m(t) and logical 0's in $\{m_k\}$ with -1 values of m(t). Specifically, we define

$$m(t) = \begin{cases} +1 & \text{for} \quad t \in [kd,\ (k+1)\,d) \quad \text{if} \quad m_k = +1 \\ -1 & \text{for} \quad t \in [kd,\ (k+1)\,d) \quad \text{if} \quad m_k = -1 \end{cases}$$

The number d is known as the digit duration and the period of m(t) is easily seen to be equal to

$$T = Ld$$

The binary waveform associated with the sequence $\{m_k\}$ illustrated above is shown in Fig. 1.

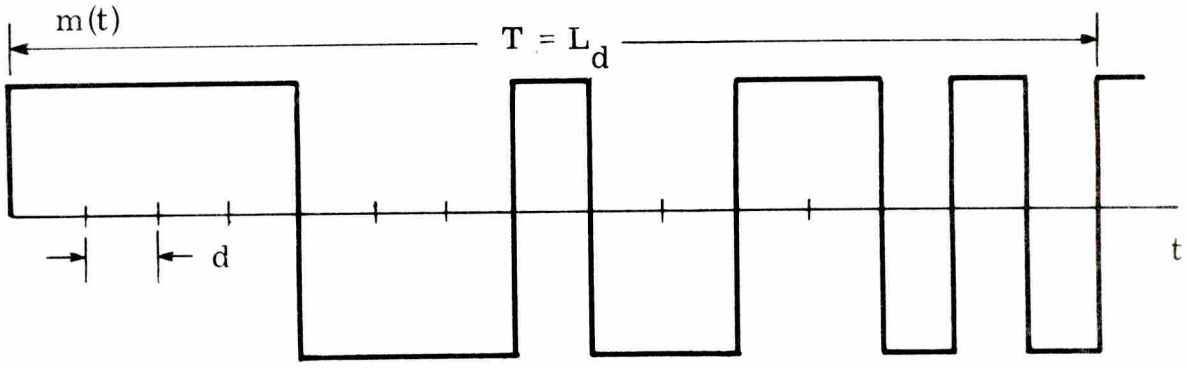

Fig. 1. One period of a LMSR binary waveform

The utility of LMSR waveforms as modulation waveforms is due to the form of the autocorrelation function

$$R_m(\tau) = \frac{1}{T} \int_0^T m(t)\, m^*(t+\tau)\, dt \qquad (1)$$

and the corresponding power spectra

$$S_m(f) = \int_{-\infty}^{\infty} R_m(\tau)\, e^{-j2\pi f}\, d\tau \qquad (2)$$

In Ref. 2 it is shown that $R_m(\cdot)$ is periodic with period T and for $\tau \in [-T/2, T/2]$,

$$R_m(\tau) = \begin{cases} 1 - \dfrac{(1+L)}{L} \dfrac{|\tau|}{d} & |\tau| \leqq d \\ -\dfrac{1}{L} & \text{otherwise} \end{cases}$$

Moreover, the power spectra for $m(t)$ is a line spectra given by,

$$S_m(f) = A(f)\, P(f) \left[\sum_n \delta(f - n/T)\right] \qquad (3)$$

where

$$P(f) = \left[\frac{\sin \pi df}{\pi df}\right]^2$$

and

$$A(f) = \begin{cases} 1/L^2 & f = 0 \\ (1+L)/L^2 & f \neq 0 \end{cases}$$

Illustrations of $R_m(\tau)$ and the root-mean-squared (RMS) power spectrum, $[S_m(f)]^{\frac{1}{2}}$, appear in Fig. 2.

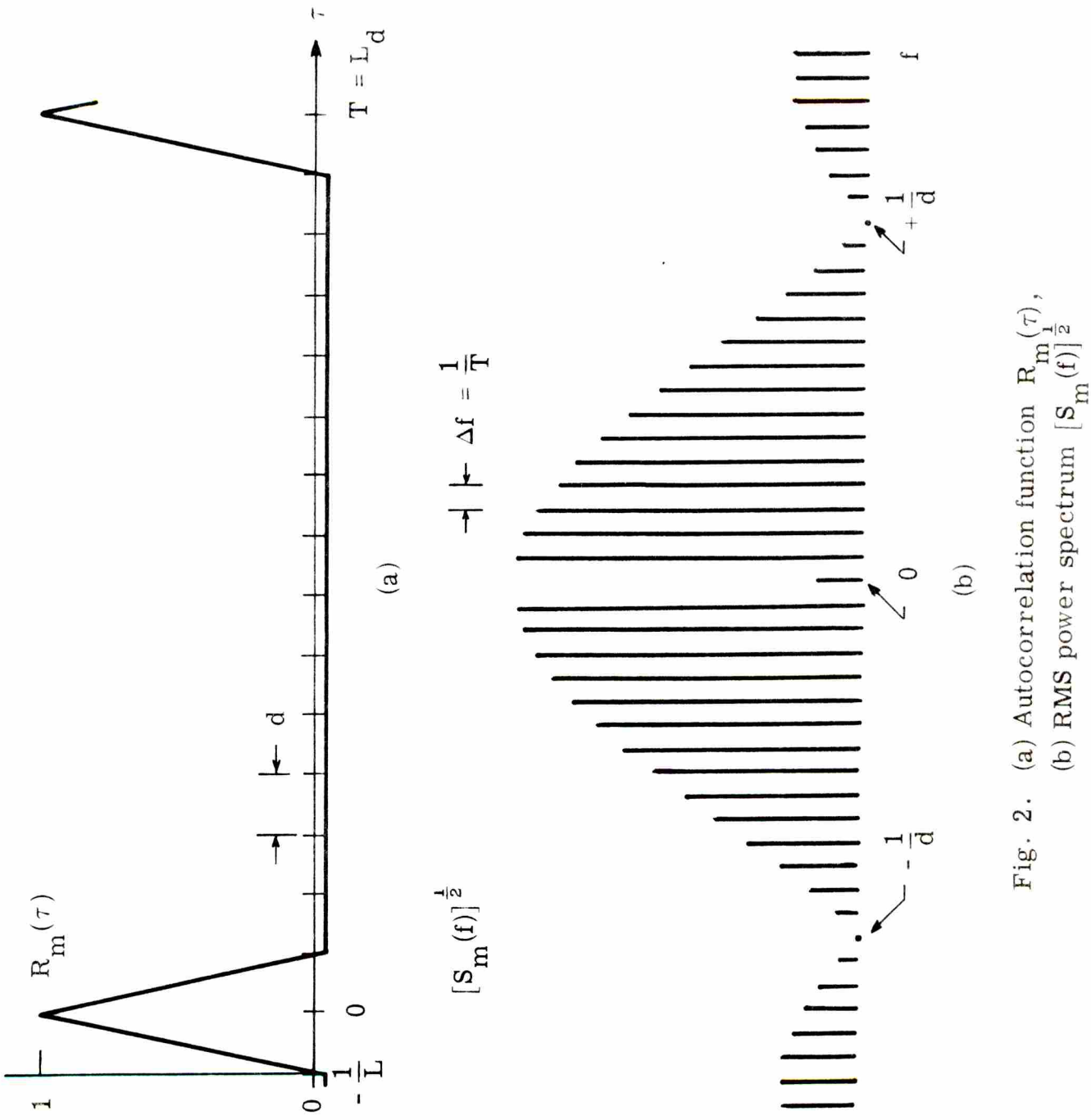

Fig. 2. (a) Autocorrelation function $R_m(\tau)$,
(b) RMS power spectrum $[S_m(f)]^{\frac{1}{2}}$

3. AMPLITUDE MODULATION, BIPHASE MODULATION AND COMPLEMENT-PHASE MODULATION

The basic idea behind LMSR modulation is to cause either the amplitude or the phase of a carrier to switch between two values depending on the value of the modulating waveform $m(t)$. In the case of amplitude modulation (AM), the amplitude switches between $+1$ and 0, in biphase modulation (BM), the phase switches between $+\pi/2$ and $-\pi/2$ and in complement-phase modulation (CM), the phase switches between $+\pi/4$ and $-\pi/4$. More precisely, if $\hat{s}(t)$ is the low-pass waveform associated with the modulated signal $s(t)$,

$$s(t) = \mathrm{Re}\left[\hat{s}(t)\left(\sqrt{2}\ e^{-j2\pi f_c t}\right)\right] \tag{4}$$

then for AM

$$\begin{aligned} s_a(t) &= \{[1 + m(t)]/2\}\ \sqrt{2}\ \sin(2\pi f_c t) \\ \hat{s}_a(t) &= [1 + m(t)]\ j/2 \end{aligned} \tag{5}$$

and for BM

$$\begin{aligned} s_b(t) &= m(t)\ \sqrt{2}\ \sin 2\pi f_c t = \sqrt{2}\ \cos[2\pi f_c t - m(t)\ \pi/2] \\ \hat{s}_b(t) &= m(t)\ j \end{aligned} \tag{6}$$

and for CM

$$s_c(t) = \sqrt{2} \cos [2\pi f_c t - m(t)\, \pi/4]$$
$$\hat{s}_c(t) = [1 + m(t)\, j] / \sqrt{2} \qquad (7)$$

In each of the above cases, it is assumed that there is an integral number of cycles of carrier for each digit in $m(t)$. If this number is denoted by D, then $s(t)$ is periodic with period

$$T = dL$$

where $$d = D/f_c$$

The complex low-pass signals for each of the three cases are illustrated in Fig. 3 and portions of the modulated waveforms appear in Fig. 4.

In order to obtain the power spectra for the three different modulation schemes, the autocorrelation functions for the low-pass signals must first be determined. These functions may be determined from the definition of the autocorrelation of a complex signal (Eq. 1) by a straightforward computation. The results are,

for AM

$$R_a(\tau) = [(1 + 2/L) + R_m(\tau)]/4 \qquad (8)$$

for BM

$$R_b(\tau) = R_m(\tau) \qquad (9)$$

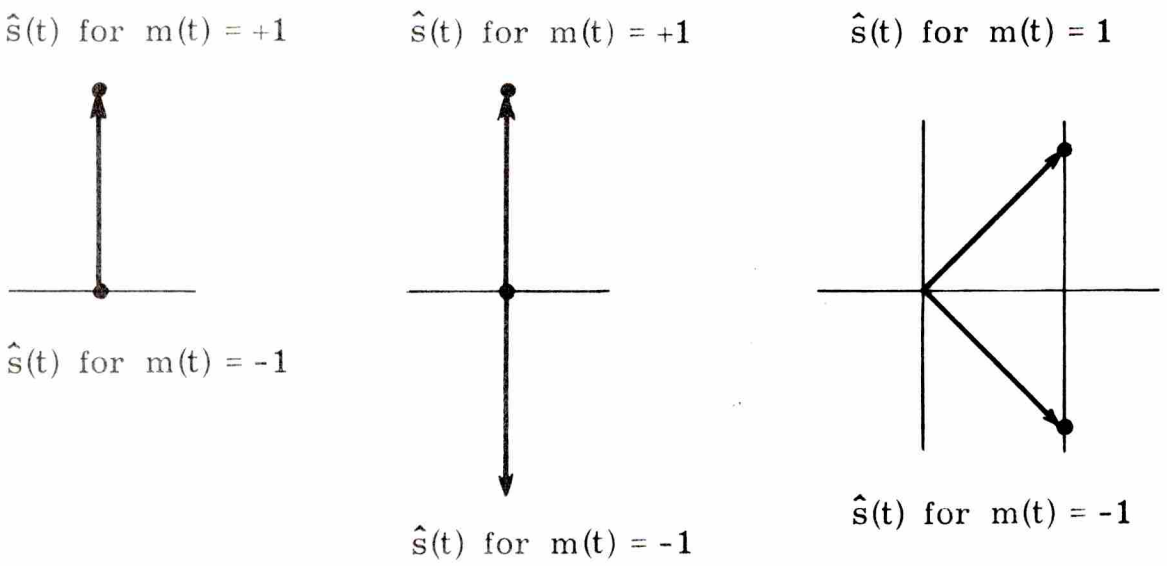

Fig. 3. The low-pass waveform $\hat{s}(t)$;
(a) AM, (b) BM, (c) CM

and for CM

$$R_c(\tau) = [1 + R_m(\tau)]/2 \tag{10}$$

Next, the spectra for the low-pass signals are obtained as the Fourier transforms of the corresponding autocorrelation functions. We have, for AM

$$S_a(f) = [(1 + 2/L)\,\delta(f) + S_m(f)]/4 \tag{11}$$

for BM

$$S_b(f) = S_m(f) \tag{12}$$

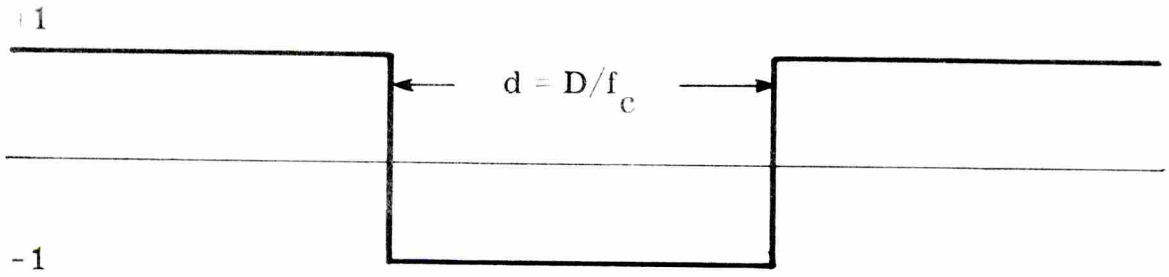

(a)

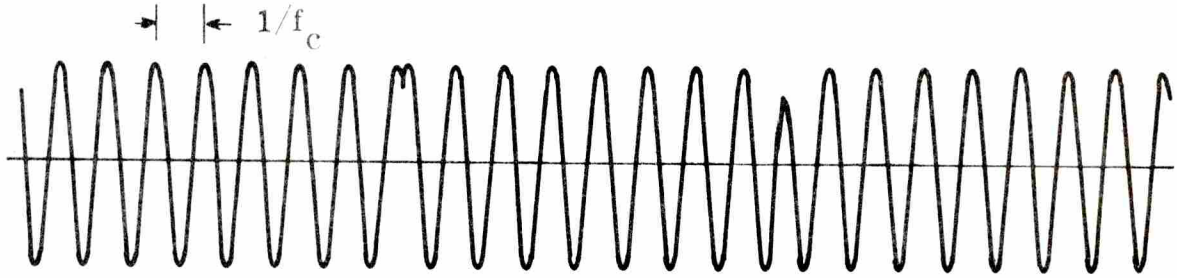

(b)

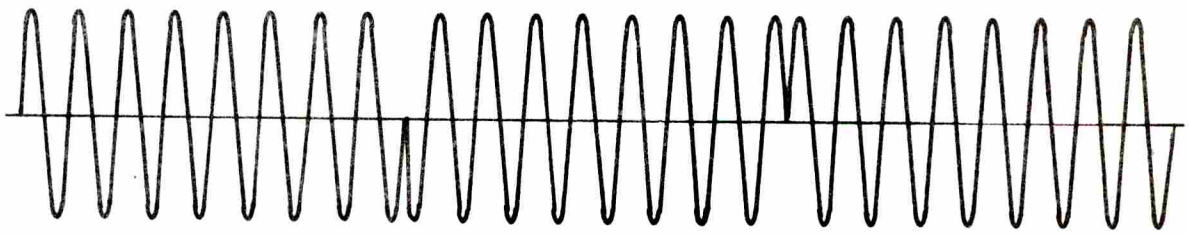

(c)

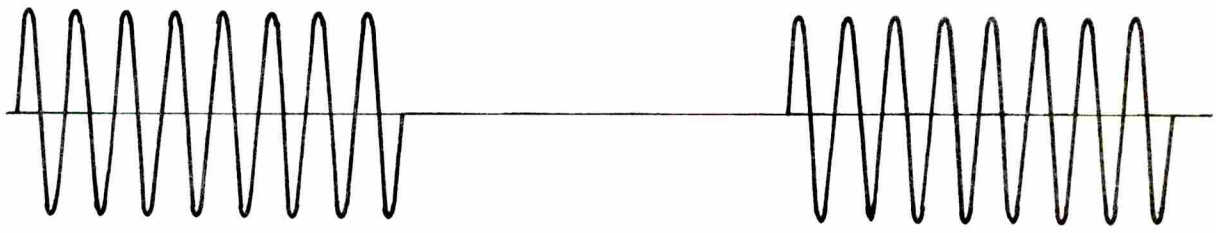

(d)

Fig. 4. The modulated signal s(t); (a) a portion of m(t), (b) CM, (c) BM, (d) AM

and for CM

$$S_c(f) = [\delta(f) + S_m(f)]/2 \tag{13}$$

or alternatively, if $\hat{S}(f)$ denotes either $S_a(f)$, $S_b(f)$ or $S_c(f)$, then

$$\hat{S}(f) = A(f)\, P(f) \sum_n (f - n/T) \tag{14}$$

where again

$$P(f) = [\sin \pi df/\pi df]^2$$

and $A(f)$ is given in Table I for the three cases.

Table I. The function $A(f)$ for AM, BM and CM

AM	$A(f) = \frac{1}{4} \frac{(1+L)^2}{L^2}$	$f = 0$
	$A(f) = \frac{1}{4} \frac{1+L}{L^2}$	$f \neq 0$
BM	$A(f) = 1/L^2$	$f = 0$
	$A(f) = \frac{1+L}{L^2}$	$f \neq 0$
CM	$A(f) = \frac{1+L^2}{2L^2}$	$f = 0$
	$A(f) = \frac{1+L}{2L^2}$	$f \neq 0$

To find the power spectrum for the modulated waveform, S(f), we note that if the number of cycles per digit, D, is larger than one, then the first zero of P(f), $d^{-1} = f_c/D$, is less than f_c. Thus, s(t) is essentially bandlimited so that,

$$S(f) = \frac{1}{2} [\hat{S}(f - f_c) + \hat{S}(f + f_c)] \tag{15}$$

Furthermore, the total average power in the modulated signal, P_S, can be obtained from the autocorrelation function of the low-pass signal by noting that,

$$P_S = \int_{-\infty}^{\infty} S(f)\, df$$

$$= \frac{1}{2} \int_{-\infty}^{\infty} [\hat{s}(f - f_c) + S(f + f_c)]\, df$$

$$= \frac{2}{2} \int_{-\infty}^{\infty} \hat{S}(f)\, df$$

or

$$P_S = \hat{R}(0) \tag{16}$$

Moreover, it is easy to show that the power in the carrier frequency line, P_c, is given by,

$$P_c = A(0) \tag{17}$$

and that the peak RMS power, P, is

$$P = \max[\hat{s}(t)] = 1 \tag{18}$$

Finally, the above equations (Eqs. 16, 17 and 18) may be used to determine the ratio of the total average power to the peak power,

$$\alpha = P_s/P = \hat{R}(0) \tag{19}$$

and the ratio of the carrier power to the total average power,

$$\beta = P_c/P_s = A(0)/\hat{R}(0) \tag{20}$$

for the three different cases. The results are summarized in Table II.

Table II. The ratios α and β for AM, BM and CM

	$\alpha = P_s/P$	$\beta = P_c/P_s$
AM	$\frac{1}{2}\left(1+\frac{1}{L}\right) \approx \frac{1}{2}$	$\frac{1}{2}\left(1+\frac{1}{L}\right) \approx \frac{1}{2}$
BM	1	$\frac{1}{L^2} \approx 0$
CM	1	$\frac{1}{2}\left(1+\frac{1}{L^2}\right) \approx \frac{1}{2}$

In the above paragraphs it has been seen that the power spectra for each of the three modulation schemes has the basic $[(\sin x)/x]^2$

form except at the carrier frequency line. The difference in the three modulation schemes appears in the ratios α and β. For a fixed peak power, the average power in the AM signal is only about half of the average power in either the BM or CM signal. On the other hand, both the AM and CM signal have approximately half of the total power contained in the carrier line, whereas the BPM signal has essentially no power contained in the carrier line.

The choice of which modulation scheme to use in a particular setting depends, of course, not only on the quantities α and β, but on the ease with which the modulation is implemented. Of the three types, AM modulation is the easiest to implement since it only involves gating the carrier on or off depending on the bits in the LMSR sequence. If more signal power is needed, however, the choice between BM and CM can be made on the basis of whether or not a large carrier power is desired, since either signal can be generated with about the same amount of difficulty. Reference 4 describes a method used to generate all three types of modulations using digital circuitry. The principle behind this method is to generate a square wave version of the modulated signal and then to filter out that portion of the spectrum centered about the harmonics of the carrier frequency. Figure 5 illustrates the output of the modulator, after being filtered by a $Q = 4$ bandpass filter.

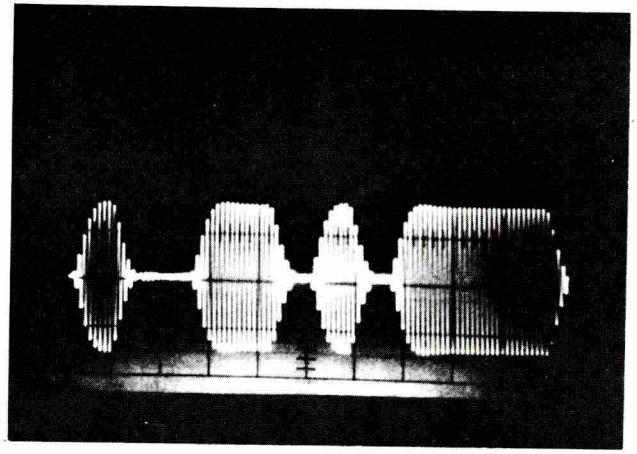

(a)

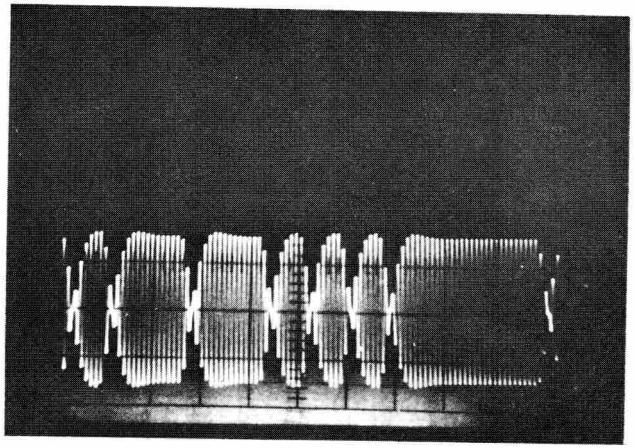

(b)

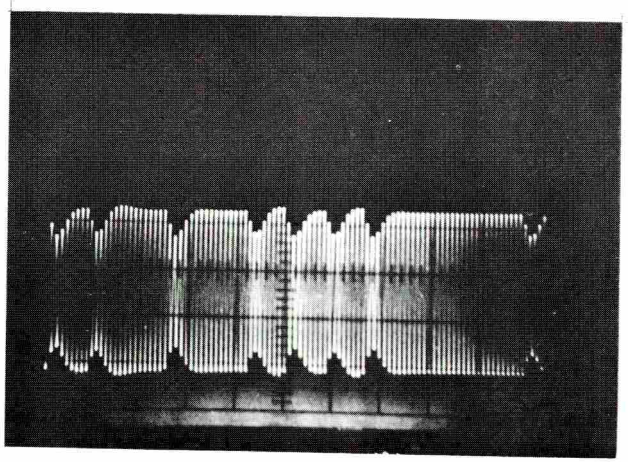

(c)

Fig. 5. The output of the digital modulator after being filtered by a Q = 4 bandpass filter (a) AM, (b) BM and (c) CM

4. A REPLICA-CORRELATION TECHNIQUE

As mentioned in the introduction, the high resolution property of repeated pulse modulation can be achieved for LMSR sequence modulation by using replica-correlation at the receiver. To be more specific, assume that the transmitted signal can be considered as being propagated over a finite number of distinct transmission paths with transient times $\tau_1, \ldots, \tau_N$ and attenuations $\alpha_1, \ldots, \alpha_N$. We may then write the demodulated reception, $r(t)$, as the sum

$$r(t) = \sum_{i=1}^{N} \alpha_i \, \hat{s}(t - \tau_i) \tag{21}$$

where $\hat{s}(\cdot)$ is the low-pass signal associated with the transmission. Now a standard technique for processing a repeated pulse transmission is to cross-correlate $r(t)$ with a replica of the pulse envelope to produce the function

$$C(\tau) = \sum_{i=1}^{N} \alpha_i \, R(\tau - \tau_i) \tag{22}$$

where $R(\cdot)$ is a triangularly shaped function with base width $2d$. From Eq. 22, it is seen that the ith transmission path appears in $C(\tau)$ as the triangular peak $R(\tau - \tau_i)$ centered at the transient time $\tau_i \pmod T$ with height proportional to the attenuation α_i. Thus, $C(\tau)$ may be used as a measure of the multipath structure of the

channel. In the following paragraphs, a replica-correlation technique is described for obtaining $C(\tau)$ when $\hat{s}(t)$ is the low-pass waveform associated with LMSR sequence modulation.

To begin, assume that a biphase modulated signal is transmitted, $[\hat{s}(t) = \hat{s}_b(t)]$, and consider the cross-correlation of $r(t)$ with the low-pass signal $\hat{s}_a(t)$. From Eq. 21, we have

$$R_{a,r}(\tau) = \frac{1}{T}\int_0^T \hat{s}_a^*(t)\, r(t+\tau)\, dt$$

$$= \frac{1}{T}\int_0^T \hat{s}_a^*(t)\left[\sum_{i=1}^{N} \alpha_i\, \hat{s}_b(t-\tau_i)\right] dt$$

$$= \sum_{i=1}^{N} \alpha_i \left[\frac{1}{T}\int_0^T \hat{s}_a^*(t+\tau-\tau_i)\, dt\right]$$

or

$$R_{a,r}(\tau) = \sum_{i=1}^{N} \alpha_i\, R_{a,b}(\tau-\tau_i) \tag{23}$$

where

$$R_{a,r}(\tau) = \frac{1}{T}\int_0^T \hat{s}_a^*(t)\, s_b(t+\tau)\, dt \tag{24}$$

But by substituting for $\hat{s}_a(t)$ and $\hat{s}_b(t)$ from Eq. 8 into Eq. 24 it is easily seen that for $|\tau| \leq T/2$

$$R_{a,b}(\tau) = \begin{cases} (1 + 1/L)\left(1 - \dfrac{|\tau|}{d}\right) & |\tau| \leq d \\ 0 & \text{otherwise} \end{cases} \tag{25}$$

Thus, $R_{a,b}(\tau)$ is a triangularly shaped function with base width $2d$ and height $1 + 1/L$. [Note that the graph of $R_{a,b}(\tau)$ can be obtained by adding $1/L$ to the graph of $R_b(\tau)$ in Fig. 2(a).] It then follows from Eq. 23 that if a biphase modulated signal is transmitted, we may determine $C(\tau)$ as

$$C(\tau) = R_{a,r}(\tau) \tag{26}$$

Next, consider the result of transmitting either an amplitude-modulated signal or a complement-phase modulated signal and again cross-correlating the demodulated reception with a replica of $\hat{s}_a(t)$. If the low-pass transmitted signal is denoted by $\hat{s}(t)$, then by proceeding as before, we have,

$$R_{a,r}(\tau) = \sum_{i=1}^{N} \alpha_i R_{a,\hat{s}}(\tau - \tau_i) \tag{27}$$

where

$$R_{a,\hat{s}}(\tau) = \frac{1}{T} \int_0^T \hat{s}_a^*(t)\, \hat{s}(t + \tau)\, dt \tag{28}$$

In the Appendix it is shown that $R_{a,\hat{s}}(\tau)$ can be written as

$$R_{a,\hat{s}}(\tau) = C_1 R_{a,b}(\tau) + C_2 \tag{29}$$

where C_1 and C_2 are constants depending on whether $\hat{s}(t)$ is an AM signal or a CM signal. Thus, we may substitute for $R_{a,\hat{s}}(\tau)$ from Eq. 29 into Eq. 27 to obtain

$$R_{a,r}(\tau) = \sum_{i=1}^{N} \alpha_i [C_1 R_{a,b}(\tau - \tau_i) + C_2]$$

or

$$R_{a,r}(\tau) = C_1 \left[\sum_{i=1}^{N} \alpha_i R_{a,b}(\tau - \tau_i)\right] + C_2 \left[\sum_{i=1}^{N} \alpha_i\right] \tag{30}$$

Next note that the first bracketed term on the right-hand side of Eq. 30 is equal to $C(\tau)$ so that Eq. 30 may be rearranged to give,

$$C(\tau) = C_1^{-1} \left\{R_{a,r}(\tau) - C_2 \left[\sum_{i=1}^{N} \alpha_i\right]\right\} \tag{31}$$

It remains to find an expression for

$$\sum_{i=1}^{N} \alpha_i$$

in terms of a measurable quantity. To this end, consider the mean of the received signal

$$R_{1,r}(\tau) = \frac{1}{T}\int_0^T r(t+\tau)\,dt$$

$$= \frac{1}{T}\int_0^T \left[\sum_{i=1}^{N} \alpha_i\, \hat{s}(t+\tau-\tau_i)\right] dt$$

$$= \sum_{i=1}^{N} \alpha_i \frac{1}{T}\int_0^T \hat{s}(t+\tau-\tau_i)\,dt$$

or, since $\hat{s}(t)$ is periodic with period T,

$$R_{1,r}(\tau) = R_{1,r} = \left[\sum_{i=1}^{N} \alpha_i\right]\left[\frac{1}{T}\int_0^T \hat{s}(t)\,dt\right] \tag{32}$$

Finally, substituting for $\left[\sum_{i=1}^{N} \alpha_i\right]$ from Eq. 32 into Eq. 31 we obtain

$$C(\tau) = A\,R_{a,r}(\tau) - B\,R_{1,r} \tag{33}$$

where

$$A = C_1^{-1}$$

$$B = [C_2/C_1]\left[\frac{1}{T}\int_0^T \hat{s}(t)\,dt\right]^{-1}$$

From Eqs. 33 and 26 it is seen that $C(\tau)$ can be determined as a linear combination of $R_{a,r}(\tau)$ and $R_{1,r}$ for each of the three modulations considered in this report. The advantage of this technique is that only the constants A and B depend on which modulation is used and thus the basic form of the receiver does not have to

be changed when the modulation is changed.

The constants A and B for the three modulations are derived in the Appendix and summarized in Table III below.

Table III. The coefficients A and B

	A	B
AM	2	$-j$
BM	1	0
CM	$\sqrt{2}$	$(-j/\sqrt{2})\,\dfrac{[1+\frac{1}{L}]}{[1+j/L]} \approx -j/\sqrt{2}$

APPENDIX

In this appendix the coefficients in Table III are derived. To this end it is first necessary to derive the coefficients in Eq. 29. We begin by noting from Eqs. 5 and 7 that

$$\hat{s}_a(t) = [j + \hat{s}_b(t)]/2 \tag{34}$$

and

$$\hat{s}_c(t) = [1 + \hat{s}_b(t)]/\sqrt{2} \tag{35}$$

For the AM case, we set $\hat{s}(t) = \hat{s}_a(t)$ in Eq. 28 and then substitute for $\hat{s}_a(t)$ from Eq. 34 to give

$$R_{a,a}(\tau) = \frac{1}{T}\int_0^T \hat{s}_a^*(t)\,\hat{s}_a(t+\tau)\,dt$$

$$= \frac{1}{T}\int_0^T \hat{s}_a^*(t)\left[\frac{j + \hat{s}_b(t+\tau)}{2}\right] dt$$

or

$$R_{a,a}(\tau) = \frac{(j)}{2}\left[\frac{1}{T}\int_0^T \hat{s}_a^*(t)\,dt\right] + \frac{1}{2}R_{a,b}(\tau) \tag{36}$$

Thus, by comparing Eq. 36 with Eq. 29 it is seen that for the AM case

$$C_1 = \frac{1}{2} \tag{37}$$

and

$$C_2 = (j/2)\left[\frac{1}{T}\int_0^T \hat{s}_a^*(t)\,dt\right] \tag{38}$$

For the CM case, we set $\hat{s}(t) = \hat{s}_c(t)$ in Eq. 28 and then substitute for $\hat{s}_c(t)$ from Eq. 35 yielding

$$R_{a,c}(\tau) = \frac{1}{T}\int_0^T \hat{s}_a^*(t)\,\hat{s}_c(t+\tau)\,dt$$

$$= \frac{1}{T}\int_0^T \hat{s}_a^*(t)\,\frac{[1+\hat{s}_b(t+\tau)]}{\sqrt{2}}\,dt$$

or

$$R_{a,c}(\tau) = \frac{1}{\sqrt{2}}\left[\frac{1}{T}\int_0^T \hat{s}_a^*(t)\,dt\right] + \frac{1}{\sqrt{2}}R_{a,b}(\tau)$$

Thus, for the CM case,

$$C_1 = \frac{1}{\sqrt{2}} \tag{39}$$

and

$$C_2 = \frac{1}{\sqrt{2}}\left[\frac{1}{T}\int_0^T \hat{s}_a^*(t)\,dt\right] \tag{40}$$

The next step in determining the constants A and B is to compute the means of the low-pass signals $\hat{s}_a(t)$ and $\hat{s}_c(t)$. From Eq. 5,

$$\frac{1}{T}\int_0^T \hat{s}_a(t)\,dt = j\left[\frac{1}{T}\int_0^T \left[\frac{1+m(t)}{2}\right] dt\right] \tag{41}$$

or

$$\frac{1}{T}\int_0^T \hat{s}_a(t)\,dt = j\left[\frac{L+1}{2}\right]\frac{1}{L} \tag{42}$$

where we have used Property 2 of Chapter 2 to evaluate the integral on the right-hand side of Eq. 41.

In a similar manner it can be shown that

$$\frac{1}{T}\int_0^T \hat{s}_c(t)\,dt = \frac{1}{T}\int_0^T \left[\frac{1+j\,m(t)}{\sqrt{2}}\right] dt$$

or

$$\frac{1}{T}\int_0^T \hat{s}_c(t)\,dt = [1+(j/L)]\frac{1}{\sqrt{2}} \tag{43}$$

Finally, the constant A_1 is determined by substituting for C_1 from Eqs. 37 and 39 into $A = 1/C_1$. The constant B, in the AM case, is given by

$$\begin{aligned} B &= \frac{C_2}{C_1}\left[\frac{1}{T}\int_0^T \hat{s}_a(t)\,dt\right]^{-1} \\ &= \frac{(j/2)}{(1/2)}\,\frac{\left[\frac{1}{T}\int_0^T \hat{s}_a{}^*(t)\,dt\right]}{\left[\frac{1}{T}\int_0^T \hat{s}_a(t)\,dt\right]} \\ &= -j \end{aligned} \tag{44}$$

and, in the CM case, by

$$B = \frac{C_2}{C_1}\left[\frac{1}{T}\int_0^T \hat{s}_c(t)\,dt\right]^{-1}$$

$$= \frac{(1/\sqrt{2})}{(1/\sqrt{2})}\,\frac{\left[\frac{1}{T}\int_0^T \hat{s}_a{}^*(t)\,dt\right]}{\left[\frac{1}{T}\int_0^T \hat{s}_c(t)\,dt\right]} \qquad (45)$$

$$= \frac{(-j/2)\,(1 + 1/L)}{(1/\sqrt{2})(1 + j/L)}$$

$$= (-j/\sqrt{2})\left[\frac{1 + 1/L}{1 + j/L}\right]$$

REFERENCES

1. T. G. Birdsall, "MIMI Processing Techniques," (Internal Memorandum), Cooley Electronics Laboratory, The University of Michigan, Ann Arbor, Michigan, December 1968.

2. S. W. Golomb, Shift Register Sequences, Chapters III and IV, Holden-Day, Inc.

3. C. C. Hoopes and R. Randall, Study of Linear Sequence Generators, Cooley Electronics Laboratory Technical Report No. 165 (6576-4-T), The University of Michigan, Ann Arbor, Michigan, June 1966.

4. J. Stewart, "Operating Principles of the ELMSG," (Internal Memorandum), Cooley Electronics Laboratory, The University of Michigan, Ann Arbor, Michigan, July 1971.

DISTRIBUTION LIST

	No. of Copies
Office of Naval Research (Code 468) (Code 102-OS) (Code 480) Navy Department Washington, D. C. 20360	1 1 1
Director, Naval Research Laboratory Technical Information Division Washington, D. C. 20390	6
Director Office of Naval Research Branch Office 1030 East Green Street Pasadena, California 91101	1
Office of Naval Research San Francisco Area Office 1076 Mission Street San Francisco, California 94103	1
Director Office of Naval Research Branch Office 495 Summer Street Boston, Massachusetts 02210	1
Office of Naval Research New York Area Office 207 West 24th Street New York, New York 10011	1
Director Office of Naval Research Branch Office 536 S. Clark Street Chicago, Illinois 60605	1
Director Naval Research Laboratory Attn: Library, Code 2029 (ONRL) Washington, D. C. 20390	8

DISTRIBUTION LIST (Cont.)

	No. of Copies
Commander Naval Ordnance Laboratory Acoustics Division White Oak, Silver Spring, Maryland 20907 Attn: Dr. Zaka Slawsky	1
Commanding Officer Naval Ship Research & Development Center Annapolis, Maryland 21401	1
Commander Naval Undersea Research & Development Center San Diego, California 92132 Attn: Dr. Dan Andrews Mr. Henry Aurand	2
Chief Scientist Navy Underwater Sound Reference Division P. O. Box 8337 Orlando, Florida 32800	1
Commanding Officer and Director Navy Underwater Systems Center Fort Trumbull New London, Connecticut 06321	1
Commander Naval Air Development Center Johnsville, Warminster, Pennsylvania 18974	1
Commanding Officer and Director Naval Ship Research and Development Center Washington, D. C. 20007	1
Superintendent Naval Postgraduate School Monterey, California 93940	1
Commanding Officer & Director Naval Ship Research & Development Center* Panama City, Florida 32402	1

*Formerly Mine Defense Lab.

DISTRIBUTION LIST (Cont.)

	No. of Copies
Naval Underwater Weapons Research & Engineering Station Newport, Rhode Island 02840	1
Superintendent Naval Academy Annapolis, Maryland 21401	1
Scientific and Technical Information Center 4301 Suitland Road Washington, D. C. 20390 Attn: Dr. T. Williams Mr. E. Bissett	2
Commander Naval Ordnance Systems Command Code ORD-03C Navy Department Washington, D. C. 20360	1
Commander Naval Ship Systems Command Code SHIPS 037 Navy Department Washington, D. C. 20360	1
Commander Naval Ship Systems Command Code SHIPS 00V1 Washington, D. C. 20360 Attn: CDR Bruce Gilchrist Mr. Carey D. Smith	2
Commander Naval Undersea Research & Development Center 3202 E. Foothill Boulevard Pasadena, California 91107	1
Commanding Officer Fleet Numerical Weather Facility Monterey, California 93940	1

DISTRIBUTION LIST (Cont.)

	No. of Copies
Defense Documentation Center Comeron Station Alexandria, Virginia 22314	20
Dr. James Probus Office of the Assistant Secretary of the Navy (R&D) Room 4E741, The Pentagon Washington, D. C. 20350	1
Mr. Allan D. Simon Office of the Secretary of Defense DDR&E Room 3E1040, The Pentagon Washington, D. C. 20301	1
CAPT J. Kelly Naval Electronics Systems Command Code EPO-3 Washington, D. C. 20360	1
Chief of Naval Operations Room 5B718, The Pentagon Washington, D. C. 20350 Attn: Mr. Benjamin Rosenberg	1
Chief of Naval Operations Rm 4C559, The Pentagon Washington, D. C. 20350 Attn: CDR J. M. Van Metre	1
Chief of Naval Operations 801 No. Randolph St. Arlington, Virginia 22203	1
Dr. Melvin J. Jacobson Rensselaer Polytechnic Institute Troy, New York 12181	1
Dr. Charles Stutt General Electric Co. P. O. Box 1088 Schenectady, New York 12301	1

DISTRIBUTION LIST (Cont.)

	No. of Copies
Dr. Alan Winder EDO Corporation College Point, New York 11356	1
Dr. T. G. Birdsall Cooley Electronics Lab. University of Michigan Ann Arbor, Michigan 48105	1
Dr. John Steinberg University of Miami Institute of Marine & Atmospheric Sciences Miami, Florida 33149	1
Mr. Robert Cunningham Bendix Corporation 11600 Sherman Way North Hollywood, California 91606	1
Dr. H. S. Hayre University of Houston Cullen Boulevard Houston, Texas 77004	1
Dr. Robert R. Brockhurst Woods Hole Oceanographic Institute Woods Hole, Massachusetts 02543	1
Dr. Stephen Wolff Johns Hopkins University Baltimore, Maryland 21218	1
Dr. M. A. Basin Litton Industries 8000 Woodley Avenue Van Nuys, California 91409	1
Dr. Albert Nuttall Navy Underwater Systems Center Fort Trumbull New London, Connecticut 06320	1

DISTRIBUTION LIST (Cont.)

	No. of Copies
Dr. Philip Stocklin Raytheon Company P. O. Box 360 Newport, Rhode Island 02841	1
Dr. H. W. Marsh Navy Underwater Systems Center Fort Trumbull New London, Connecticut 06320	1
Dr. David Middleton 35 Concord Ave., Apt. #1 Cambridge, Massachusetts 02138	1
Mr. Richard Vesper Perkin-Elmer Corporation Electro-Optical Division Norwalk, Connecticut 06852	1
Dr. Donald W. Tufts University of Rhode Island Kingston, Rhode Island 02881	1
Dr. Loren W. Nolte Dept. of Electrical Engineering Duke University Durham, North Carolina 27706	1
Dr. Thomas W. Ellis Texas Instruments, Inc. 13500 North Central Expressway Dallas, Texas 75231	1
Mr. Robert Swarts Honeywell, Inc. Marine Systems Center 5303 Shilshole Ave., N.W. Seattle, Washington, 98107	1
Mr. Charles Loda Institute for Defense Analyses 400 Army-Navy Drive Arlington, Virginia 22202	1

DISTRIBUTION LIST (Cont.)

	No. of Copies
Mr. Beaumont Buck General Motors Corporation Defense Research Division 6767 Holister Ave. Goleta, California 93017	1
Dr. M. Weinstein Underwater Systems, Inc. 8121 Georgia Avenue Silver Spring, Maryland 20910	1
Dr. Harold Saxton 1601 Research Blvd. TRACOR, Inc. Rockville, Maryland 20850	1
Dr. Thomas G. Kincaid General Electric Company P. O. Box 1088 Schenectady, New York 12305	1
Applied Research Laboratories The University of Texas at Austin Austin, Texas 78712 Attn: Dr. Loyd Hampton Dr. Charles Wood	3
Dr. Paul McElroy Woods Hole Oceanographic Institution Woods Hole, Massachusetts 02543	1
Dr. John Bouyoucos General Dynamics/ Electronics 1400 N. Goodman Street, P. O. Box 226 Rochester, New York 14603	1
Hydrospace Research Corporation 5541 Nicholson Lane Rockville, Maryland 20852 Attn: CDR Craig Olson	1
Cooley Electronics Laboratory University of Michigan Ann Arbor, Michigan 48105	25